Reproducibility and Accuracy of Quantitative Myocardial Blood Flow Assessment with ^{82}Rb PET: Comparison with ^{13}N-Ammonia PET

Georges El Fakhri[1], Arash Kardan[1], Arkadiusz Sitek[2], Sharmila Dorbala[2,3], Nathalie Abi-Hatem[1,4], Youmna Lahoud[4], Alan Fischman[5], Martha Coughlan[2], Tsunehiro Yasuda[1], and Marcelo F. Di Carli[2,3]

[1]Division of Nuclear Medicine and Molecular Imaging, Department of Radiology, Massachusetts General Hospital, Harvard Medical School, Boston, Massachusetts; [2]Division of Nuclear Medicine, Department of Radiology, Brigham and Women's Hospital, Boston, Massachusetts; [3]Cardiovascular Imaging Program, Brigham and Women's Hospital, Boston, Massachusetts; [4]Faculty of Medicine, Holy Spirit University of Kaslik, Mount Lebanon, Lebanon; and [5]Shriners Hospital for Children, Boston, Massachusetts

^{82}Rb cardiac PET allows the assessment of myocardial perfusion with a column generator in clinics that lack a cyclotron. There is evidence that the quantitation of myocardial blood flow (MBF) and coronary flow reserve (CFR) with dynamic ^{82}Rb PET is feasible. The objectives of this study were to determine the accuracy and reproducibility of MBF estimates from dynamic ^{82}Rb PET by using our methodology for generalized factor analysis (generalized factor analysis of dynamic sequences [GFADS]) and compartment analysis. **Methods:** Reproducibility was evaluated in 22 subjects undergoing dynamic rest and dipyridamole stress ^{82}Rb PET studies at a 2-wk interval. The inter- and intraobserver variability of MBF quantitation with dynamic ^{82}Rb PET was assessed with 4 repeated estimations by each of 4 observers. Accuracy was evaluated in 20 subjects undergoing dynamic rest and dipyridamole stress PET studies with ^{82}Rb and ^{13}N-ammonia, respectively. The left ventricular and right ventricular blood pool and left ventricular tissue time–activity curves were estimated by GFADS. MBF was estimated by fitting the blood pool and tissue time–activity curves to a 2-compartment kinetic model for ^{82}Rb and to a 3-compartment model for ^{13}N-ammonia. CFR was estimated as the ratio of peak MBF to baseline MBF. **Results:** The reproducibility of the MBF estimates in repeated ^{82}Rb studies was very good at rest and during peak stress (R^2 = 0.935), as was the reproducibility of the CFR estimates (R^2 = 0.841). The slope of the correlation line was very close to one for the estimation of MBF (0.986) and CFR (0.960) in repeated ^{82}Rb studies. The intraobserver reliability was less than 3% for the estimation of MBF at rest and during peak stress as well as for the estimation of CFR. The interobserver reliabilities were 0.950 at rest and 0.975 at peak stress. The correlation between myocardial flow estimates obtained at rest and those obtained during peak stress in ^{82}Rb and ^{13}N-ammonia studies was very good (R^2 = 0.857). Bland–Altman plots comparing CFR estimated with ^{82}Rb and CFR estimated with ^{13}N-ammonia revealed an underestimation of CFR with ^{82}Rb compared with ^{13}N-ammonia; the underestimation was within ±1.96 SD. **Conclusion:** MBF quantitation with GFADS and dynamic ^{82}Rb PET demonstrated excellent reproducibility as well as intra- and interobserver reliability. The accuracy of the absolute quantitation of MBF with factor and compartment analyses and dynamic ^{82}Rb PET was very good, compared with that achieved with ^{13}N-ammonia, for MBF of up to 2.5 mL/g/min.

Key Words: myocardial blood flow; PET; ^{82}Rb; ^{13}N-ammonia

J Nucl Med 2009; 50:1062–1071
DOI: 10.2967/jnumed.104.007831

PET measures of myocardial blood flow (MBF) (in mL/min/g) and coronary vasodilator reserve are very sensitive for evaluating microvascular function in vivo (*1–3*). Although the quantitation of MBF with ^{13}N-ammonia and ^{15}O-water as PET flow tracers has been validated, these tracers are seldom used clinically because they are cyclotron products with short physical half-lives (10 and 2 min, respectively) and therefore require an on-site cyclotron. In contrast, ^{82}Rb can be produced with a column generator; consequently, it is the agent most commonly used for assessing myocardial perfusion in patients with known or suspected coronary artery disease (CAD) (*4–10*). Although this approach has been shown to be highly accurate for the detection of obstructive CAD (*11,12*), it underestimates the extent of underlying CAD, especially in patients with multivessel disease. This limitation could be overcome by adding the quantification of MBF to routine visual or semiquantitative assessments of myocardial perfusion.

We and others have shown that the absolute quantitation of MBF and coronary flow reserve (CFR) with dynamic ^{82}Rb PET is feasible in humans (*7–10,13,14*). However, little is known about the accuracy and reproducibility of this approach to estimating MBF. Accordingly, we sought to determine the reproducibility of MBF estimates with ^{82}Rb PET as well as the intra- and interobserver reliability of these quantitative measures. In addition, we determined the accuracy of the quantitative ^{82}Rb PET approach by

Received Aug. 13, 2008; revision accepted Mar. 23, 2009.
For correspondence or reprints contact: Georges El Fakhri, Division of Nuclear Medicine and Molecular Imaging, Department of Radiology, Massachusetts General Hospital, 55 Fruit St., Boston, MA 02114.
E-mail: elfakhri@pet.mgh.harvard.edu

comparing measures of MBF obtained with ^{82}Rb and those obtained with ^{13}N-ammonia.

MATERIALS AND METHODS

Study Population

Two separate groups of subjects were recruited for the reproducibility and accuracy studies. We included patients at risk for or with known CAD, defined by the presence of fixed or reversible perfusion defects on clinically indicated PET. We also included healthy volunteers with a low likelihood of obstructive CAD, on the basis of the absence of chest pain and coronary risk factors and a normal resting electrocardiogram. Subjects who were pregnant or breast-feeding were excluded, as were those with uncontrolled hypertension (>200/120 mm Hg), unstable coronary syndromes, significant cardiac arrhythmias, valvular heart disease, decompensated congestive heart failure, bronchospastic pulmonary disease, or known hypersensitivity to dipyridamole.

Study Design

The Institutional Review Board of Partners Healthcare System, Boston, MA, approved the study protocol, and all participants gave written informed consent. Each subject made 2 hospital visits (visits 1 and 2), during which rest and dipyridamole stress myocardial perfusion was assessed. In the reproducibility study, all subjects underwent rest and dipyridamole stress myocardial perfusion PET studies with ^{82}Rb as the flow agent at a 2-wk interval. In the accuracy study, all subjects underwent separate rest and dipyridamole stress myocardial perfusion PET studies with ^{82}Rb and ^{13}N-ammonia, respectively, also at a 2-wk interval.

PET

All subjects refrained from using caffeine-containing beverages or theophylline-containing medications for 24 h before each PET scan. Vasoactive medications were withheld for 24 h before the study. All subjects were studied in the fasting state.

^{82}Rb PET. All ^{82}Rb studies were performed in the 2-dimensional mode with a whole-body PET/CT scanner (Discovery STE Lightspeed 64; GE Healthcare). Myocardial perfusion was assessed at rest and during vasodilator stress with dipyridamole. Initial scout (120 kVp; 10 mA) and transmission (140 kVp; 10 mA) CT scans were obtained for orientation and attenuation correction. Beginning with the intravenous bolus administration of 1,850 MBq (~50 mCi) of ^{82}Rb (Bracco Diagnostics) in 14 ± 6 (mean ± SD) mL of saline, serial images were acquired for ~6 min (fourteen 5-s images, six 10-s images, three 20-s images, three 30-s images, and one 90-s image). Immediately after completion of the rest study, a standard intravenous dipyridamole infusion (0.142 mg/kg/min) was administered for 4 min. Three minutes after termination of the dipyridamole infusion, a second dose of 1,850 MBq (~50 mCi) of ^{82}Rb was injected, and dynamic PET images were acquired in the same fashion. A second CT transmission scan (140 kVp, 10 mA) was then acquired for attenuation correction of the stress images. The heart rate, systemic blood pressure, and 12-lead electrocardiogram were recorded at baseline and throughout the infusion of dipyridamole. The rate × pressure product (RPP) was calculated as the heart rate multiplied by the systolic blood pressure.

The attenuation map used for correction of the 511-keV photon attenuation was derived from the CT scan by use of a continuous conversion scale with a range of slopes dependent on the CT kilovoltage and number of scans (*15*). Randoms correction was performed by direct subtraction of delayed events, and scatter correction was performed with the scatter correction approach proposed by Bergstrom et al. (*16*). All dynamic sinograms were reconstructed with attenuation-weighted ordered-subset expectation maximization (21 subsets and 2 iterations, as recommended by the manufacturer of the scanner) into 26 dynamic frames, each with a volume of 128 × 128 × 47 voxels. No postfiltering was performed.

^{13}N-Ammonia PET. All ^{13}N-ammonia studies were performed in the 2-dimensional mode with a whole-body PET scanner (PC-2048 Scanditronix; GE Healthcare). A 10-min transmission scan was first acquired for the correction of photon attenuation. Beginning with the intravenous bolus administration of ^{13}N-ammonia at 925 MBq (25 mCi), serial images were acquired over 19 min (thirty 6-s images and then eight 120-s images). Thirty minutes later, a second transmission scan was obtained to ensure correct positioning of the patient and attenuation correction during stress. Next, intravenous dipyridamole (0.142 mg/kg/min) was infused for 4 min. Three minutes after completion of the dipyridamole infusion, a second dose of 925 MBq (25 mCi) of ^{13}N-ammonia was injected, and images were recorded with the same acquisition sequence. The heart rate, systemic blood pressure, and 12-lead electrocardiogram were recorded at baseline and throughout the infusion of dipyridamole. The RPP was calculated as the heart rate multiplied by the systolic blood pressure.

The attenuation map used for correction of the 511-keV photon attenuation was measured at 511 keV with a ^{68}Ge source. Randoms correction was performed by subtraction of delayed events, and scatter correction was performed with the scatter correction approach proposed by Bergstrom et al. (*16*). All dynamic sinograms were reconstructed with a filtered backprojection clinical protocol (recommended by the manufacturer of the scanner) into 38 dynamic frames, each with a volume of 128 × 128 × 47 voxels. No postfiltering was performed.

Quantification of MBF

All reconstructed dynamic PET data were analyzed with quantitative dynamic analysis software, which we previously developed and reported (*14,17*). The software uses generalized factor analysis of dynamic sequences (GFADS), an approach that addresses the nonuniqueness problem in cardiac PET (*14,18*) by penalizing spatial overlap between factor images, to sample the right ventricular (RV) and left ventricular (LV) blood pools and the LV myocardium to derive the blood pool and tissue time–activity curves for both the ^{82}Rb and the ^{13}N-ammonia studies as described previously (*14*).

In brief, GFADS was performed and then overlap between factor images was eliminated by modifying the factors and factor images obtained in the first step to minimize the nonnegative term that penalizes the overlap between images of factor coefficients while keeping the matrix product of factor and factor images constant. Therefore, the time–activity curve in each voxel was modeled as a combination of 3 contributions: the contribution from myocardial tissue, modeled with compartment analysis, and contributions from RV and LV blood pools, modeled as fractions of measured LV and RV input functions. Figure 1 shows typical factors and corresponding factor images associated with ^{82}Rb and ^{13}N-ammonia dynamic studies in the same subject. Note that the LV and RV input functions are obtained automatically as the LV and RV factors estimated for the whole factor image, as opposed to a region of interest.

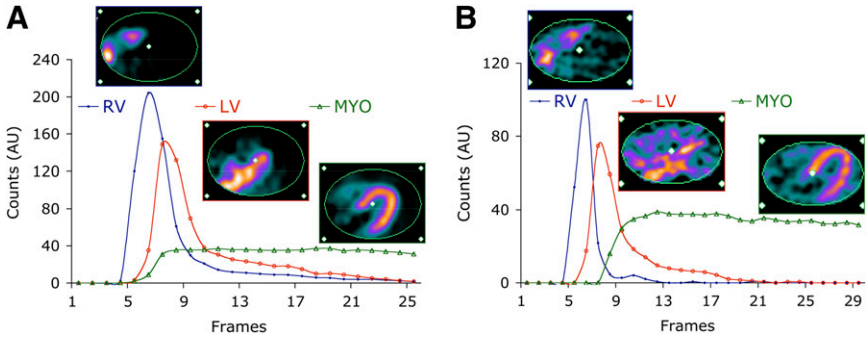

FIGURE 1. Typical factors and corresponding factor images associated with ^{82}Rb (A) and ^{13}N-ammonia (B) dynamic studies in same subject. AU = arbitrary units; MYO = whole myocardium.

Next, kinetic analysis was performed as described later. The user input consisted of choosing the parameters of the kinetic model (such as type of study [^{13}N ammonia or ^{82}Rb] and number of compartments). The result was a parametric 17-segment polar map (*19*). The 3 main coronary arteries (left anterior descending artery [LAD], left circumflex coronary artery [LCX], and right coronary artery [RCA]) were overlaid on the polar map to allow direct reading of the mean flow in each coronary territory.

Tracer Kinetic Model

MBF for ^{82}Rb was obtained by fitting the ^{82}Rb time–activity curves to a 2-compartment kinetic model as described previously (*20*). The 2 compartments of the model are the "free rubidium space" (blood perfusing the myocardium and the interstitial space) and the "trapped rubidium space" (myocardium). The main parameters of the model are the kinetic transport constants K_1 (mL/min/g) and k_2 (min^{-1}), which denote the extraction (forward) and egress (backward) rates of transport between the metabolically trapped space (myocardium) and the freely diffusible space (blood pool), respectively. To estimate MBF from measures of K_1, we used the extraction fraction (E) reported previously for an open-chest procedure on dogs by Yoshida et al. (*21*):

$$E = \frac{K_1}{MBF} = 1 - e^{-(0.45+0.16MBF)/MBF}. \quad \text{Eq. 1}$$

Equation 1 was solved for MBF by use of the fixed-point iteration approach (*22*). Because the equation does not have a solution for high MBF values, we used the following linear extrapolation for K_1 values of greater than 0.92 mL/g/min to allow for extraction fractions for flow values of greater than 3.7 mL/g/min while ensuring continuity of the function:

$$MBF = 3.664 + (K_1 - 0.92). \quad \text{Eq. 2}$$

The tissue time–activity curve in each voxel, $C_T(t)$, was modeled as a combination of 3 contributions: the contribution from myocardial tissue, modeled with the 2-compartment model, and contributions from LV and RV cavities, modeled as fractions of measured LV and right RV input functions:

$$C_{T_i}(t) = f_v^i C_a(t) + r_v^i C_r(t) + (1 - f_v^i - r_v^i) C_a(t) \otimes K_1^i \exp(-k_2^i t), \quad \text{Eq. 3}$$

where $C_{T_i}(t)$ is the value at time t for polar map sector i ($1 \le i \le 17$); C_{T_i} is the time–activity curve for sector i; $C_a(t)$ is the measured LV input function; $C_r(t)$ is the measured RV input function; and K_1^i, k_2^i, f_v^i, and r_v^i are the kinetic parameters for sector i, where K_1^i (mL/min/g) characterizes myocardial tissue extraction (inflow), k_2^i (min^{-1}) characterizes myocardial tissue egress (outflow), f_v^i (dimensionless) represents the contribution to the total activity from the blood input function $C_a(t)$, and r_v^i (dimensionless) represents the contribution from the activity in the RV [$C_r(t)$], which differs, in general, from the input function $C_a(t)$.

For ^{13}N-ammonia, MBF was obtained by fitting the ^{13}N-ammonia time–activity curves to a previously validated 3-compartment model (*2*). The 3 compartments assumed in the model are arterial blood, the interstitial and free cellular space, and the metabolic space. The activity concentration in LV arterial blood is denoted $C_a(t)$, that in RV arterial blood is denoted $C_r(t)$, that in the interstitial and free cellular space is denoted $C_E(t)$, and that in the metabolic space is denoted $C_G(t)$. We denoted $C_{T_i}(t)$ as the value of the tissue time–activity curve at time t in polar map sector i ($1 \le i \le 17$). The formalism used for ^{82}Rb was also used for ^{13}N-ammonia; that is, K_1^i(mL/g/min), k_2^i(1/min), and k_3^i(1/min) were used as the kinetic parameters for the ^{13}N-ammonia compartment model. The tissue time–activity curve, $C_{T_i}(t)$, can be expressed as:

$$C_{T_i}(t) = f_v^i C_a(t) + r_v^i C_r(t) + (1 - f_v^i - r_v^i)(C_{E_i}(t) + C_{G_i}(t)), \quad \text{Eq. 4}$$

where $f_v^i$and r_v^i correspond to the fractions of LV input and LR input in the tissue and, therefore, model the vascular fraction in the tissue and the spillover from the left and right ventricles. Differential equations corresponding to the kinetic model were solved with the fourth-order Runge–Kutta approach (*23*). Nonlinear optimization of the kinetic parameters (K_1^i, k_2^i, k_3^i, f_v^i, and r_v^i) was performed with the Marquardt least squares method. As validated and reported by Muzik et al. (*2*), the extraction fraction for the range of blood flow values in the present study was assumed to be one. Thus, blood flow was calculated as the value for K_1^i.

Intra- and Interobserver Reliability

The estimation of MBF was performed by 4 independent observers to assess interobserver variability, and MBF was estimated separately 4 times to assess intraobserver variability. All observers were instructed with a separate teaching dataset on how to follow the same rules in selecting a large volume of interest encompassing the heart to perform factor and compartment analyses and to perform oblique rotations into a short axis and vertical and horizontal long axes to estimate a polar map. The compartment analysis was performed for each sector of the polar map. The mean estimates for the 4 measurements of flow at rest and flow during stress were used to assess the variability intro-

duced by the factor and compartment analyses. Finally, the reproducibility of the ^{82}Rb imaging itself was assessed by comparing MBF measured at rest and MBF measured during peak stress at visits 1 and 2.

Statistical Analyses

The Spearman (ρ) nonparametric correlation coefficient (*24*) was used to assess the reproducibility of MBF quantitation by ^{82}Rb PET at visits 1 and 2 and for comparison of MBF estimates obtained with ^{82}Rb and ^{13}N-ammonia. Bland–Altman plots of the residuals (difference between mean MBF values in repeated ^{82}Rb studies or in ^{82}Rb and ^{13}N-ammonia studies) against the means were also constructed to assess any systematic error or bias (*25,26*).

The intraobserver variability in estimating MBF with ^{82}Rb was assessed by averaging all 4 estimates of MBF made by each observer and computing the coefficient of repeatability for the GFADS and the compartment analysis in the rest and stress studies. The interobserver reliability was assessed by computing the average measured intraclass correlation among the 4 observers (and applying the Spearman–Brown correction) by use of a 2-way mixed-effects model with absolute agreement definition and then computing the interrater reliability coefficient. The interobserver variability in estimating MBF with ^{82}Rb was assessed with the Spearman (ρ) nonparametric correlation coefficient (*24*). A P value of less than 0.05 was used to define statistical significance.

RESULTS

Study Population and Systemic Hemodynamics

Table 1 summarizes the characteristics of the study population for the reproducibility and accuracy portions of the study. The reproducibility cohort consisted of 20 healthy volunteers and 22 subjects (11 men and 11 women; mean age, 48 y) who were at risk for CAD (n = 2), as evidenced by the presence of coronary risk factors (such as prior myocardial infarct or CAD), or who had prior CAD (n = 1). Twenty subjects (12 women and 8 men; mean age, 34 y) participated in the accuracy study and included 19 healthy volunteers and 1 subject at risk for CAD with prior CAD.

Table 2 summarizes the systemic hemodynamics of the study cohorts. The resting heart rate, systolic blood pressure, mean arterial blood pressure, and RPP were similar in both PET studies for each study cohort. During dipyridamole stress, the heart rate and the RPP increased similarly, whereas the blood pressure remained unchanged in both study cohorts.

TABLE 1. Characteristics of Study Cohorts

Characteristic	Reproducibility (n = 22)	Accuracy (n = 20)
Age (y)	48.0 ± 12.3	34.3 ± 11.6
Female/male ratio	11/11	12/8
Hypertension	4	1
Diabetes	2	0
Smoking	1	3
Dyslipidemia	5	4
Prior CAD	1	0
Prior MI	1	0
Chest pain	1	0
Chronic obstructive pulmonary disease	0	0

Data are reported as number of subjects unless otherwise indicated.

TABLE 2. Per-Patient Analysis of Systemic and Coronary Hemodynamics

Parameter	Reproducibility (mean ± SD, n = 22)		Accuracy (mean ± SD, n = 20)	
	^{82}Rb study 1	^{82}Rb study 2	^{82}Rb	^{13}N ammonia
Systemic hemodynamics				
HR at rest	65 ± 8	65 ± 9	64 ± 11	60 ± 9
Systolic BP at rest	135 ± 17	134 ± 16	126 ± 21	108 ± 8
Mean arterial BP at rest	91 ± 11	92 ± 21	84 ± 14	80 ± 13
RPP at rest	8,682 ± 1,368	8,717 ± 1,575	8,100 ± 2,423	6,588 ± 1,056
Peak HR	80 ± 14	83 ± 11	82 ± 16	87 ± 24
Peak systolic BP	139 ± 23	127 ± 20	124 ± 19	110 ± 16
Peak mean arterial BP	93 ± 15	84 ± 16	81 ± 13	73 ± 31
Peak RPP	11,053 ± 2,657	10,414 ± 2,137	10,165 ± 2,373	9,586 ± 2,976
Coronary hemodynamics				
MBF at rest	1.13 ± 0.19	1.09 ± 0.18	0.83 ± 0.15	0.61 ± 0.14
MBF at rest, corrected	1.18 ± 0.32	1.15 ± 0.27	0.91 ± 0.23	0.79 ± 0.22
Peak MBF during stress	2.81 ± 1.02	2.71 ± 1.11	1.72 ± 0.41	1.92 ± 0.28
CFR	2.51 ± 0.89	2.40 ± 0.96	2.00 ± 0.67	2.58 ± 0.68
CVR at rest	84.8 ± 23.5	85.1 ± 28.8	103.2 ± 44.7	102.1 ± 34.1
Peak CVR during stress	37.8 ± 16.0	36.9 ± 17.45	51.4 ± 19.6	41.9 ± 4.2

HR = heart rate, in bpm; BP = blood pressure, in mm Hg; CVR = coronary vascular resistance, which is calculated as mean arterial BP/MBF and reported in mm Hg/mL/g/min.

RPP is calculated as heart rate (in bpm) × systolic blood pressure (in mm Hg). MBF is reported in mL/g/min. CFR is calculated as peak MBF during stress/MBF at rest.

TABLE 3. Per–Vascular Territory Analysis of Reproducibility of MBF, CFR, and Coronary Vascular Resistance (CVR)

Parameter	^{82}Rb visit 1			^{82}Rb visit 2		
	LAD	LOX	RCA	LAD	LOX	RCA
MBF at rest	0.86 ± 0.16	0.89 ± 0.15	0.90 ± 0.18	0.83 ± 0.15	0.85 ± 0.15	0.87 ± 0.14
MBF at rest, corrected	0.91 ± 0.22	0.94 ± 0.20	0.95 ± 0.23	0.90 ± 0.23	0.92 ± 0.22	0.94 ± 0.20
Peak MBF during stress	1.87 ± 0.72	1.86 ± 0.66	1.92 ± 0.77	1.80 ± 0.63	1.84 ± 0.64	1.86 ± 0.64
CFR	2.10 ± 0.76	2.00 ± 0.61	2.09 ± 0.79	2.03 ± 0.65	2.04 ± 0.70	1.99 ± 0.61
CVR at rest	108.36 ± 34.74	103.84 ± 30.10	105.80 ± 38.63	110.04 ± 40.24	107.52 ± 39.99	104.56 ± 40.40
Peak CVR during stress	56.83 ± 23.35	56.17 ± 21.76	55.19 ± 21.38	53.16 ± 26.50	51.48 ± 24.04	50.42 ± 21.35

Data are reported as mean ± SD. MBF is reported in mL/g/min. CFR is calculated as peak MBF during stress/MBF at rest. CVR is calculated as mean arterial blood pressure/MBF and reported in mm Hg/mL/g/min.

MBF, CFR, and Coronary Vascular Resistance

Per-Patient Analysis. The baseline MBF was regionally homogeneous and similar in the 2 PET studies performed for each subject in the reproducibility and accuracy cohorts (Table 2). During hyperemia, blood flow increased and coronary vascular resistance decreased homogeneously and significantly ($P < 0.05$, as determined with paired Student t test) in the 2 PET studies performed for each subject in the reproducibility and accuracy cohorts (Table 2). RPP-normalized rest MBF and peak stress MBF in subjects enrolled in the reproducibility study were not significantly different from those in subjects enrolled in the accuracy study (Table 2). Consequently, estimates of coronary vasodilator reserve in subjects in the reproducibility study were not statistically significantly different from those in subjects in the accuracy study (Table 2).

Per–Vascular Territory Analysis. Tables 3 and 4 show the rest and peak stress mean MBF values in the 3 main coronary territories (LAD, LCX, and RCA) as well as the CFR obtained with repeated ^{82}Rb PET scans in the reproducibility study and with ^{82}Rb and ^{13}N-ammonia in the accuracy study. No statistically significant differences were observed at the level of $P < 0.05$ in any of the LAD, LCX, or RCA territories in repeated ^{82}Rb studies at rest or during peak stress or when estimating the CFR. Figure 2 shows a typical example of ^{82}Rb and ^{13}N-ammonia stress studies performed in the same subject. Transverse, coronal, and sagittal slices as well as short-axis, vertical-long-axis (VLA), and horizontal-long-axis (HLA) are shown along with polar maps of relative perfusion and absolute MBF in the typical display of our quantitation software. Note the lower spatial resolution in the ^{82}Rb PET study than in the ^{13}N-ammonia PET study, mainly because of the greater positron range of ^{82}Rb (full width at half maximum, 1.6 mm) than of ^{13}N-ammonia (~0.28 mm).

Intra- and Interobserver Reliability

Figure 3 shows the intraobserver and GFADS variability of the estimation of MBF at rest and MBF during stress, which can be imputed to factor and compartment analyses and, to a lesser extent, to observer variability because the processing was fully automated—except for the choice of the volume of study and the quality control of the polar map generation. Similar results were obtained for the reproducibility of the estimation of CFR. Our results indicated excellent reproducibility of our quantitative dynamic ^{82}Rb approach based on factor and compartment analyses for the estimation of MBF ($R^2 = 0.99$) and CFR ($R^2 = 0.97$). The coefficients of repeatability for the estimation of MBF at rest, MBF during peak stress, and CFR were 1.7%, 1.4%, and 2.8%, respectively.

The interobserver variability among the 4 observers who participated in the present study is shown in Figure 4 for the estimation of CFR. Similar results were obtained for the estimation of MBF at rest and MBF during stress. The interobserver variability between any 2 observers for the

TABLE 4. Per–Vascular Territory Analysis of Accuracy of MBF, CFR, and Coronary Vascular Resistance (CVR)

Parameter	^{82}Rb			^{13}N-ammonia		
	LAD	LOX	RCA	LAD	LOX	RCA
MBF at rest	0.80 ± 0.13	0.82 ± 0.18	0.88 ± 0.18	0.61 ± 0.14	0.62 ± 0.18	0.60 ± 0.16
MBF at rest, corrected	0.90 ± 0.24	0.91 ± 0.25	0.98 ± 0.25	0.78 ± 0.22	0.81 ± 0.29	0.77 ± 0.22
Peak MBF during stress	1.70 ± 0.37	1.66 ± 0.36	1.82 ± 0.50	1.97 ± 0.33	1.89 ± 0.29	1.90 ± 0.30
CFR	2.01 ± 0.69	1.93 ± 0.65	1.97 ± 0.76	2.66 ± 0.72	2.55 ± 0.77	2.60 ± 0.64
CVR at rest	105.88 ± 48.38	103.95 ± 45.80	97.22 ± 44.38	102.88 ± 34.05	100.28 ± 36.87	106.92 ± 37.14
Peak CVR during stress	52.29 ± 20.88	52.86 ± 18.61	49.74 ± 19.86	40.48 ± 2.92	43.01 ± 5.17	42.41 ± 5.49

Data are reported as mean ± SD. MBF is reported in mL/g/min. CFR is calculated as peak MBF during stress/MBF at rest. CVR is calculated as mean arterial blood pressure/MBF and reported in mm Hg/mL/g/min.

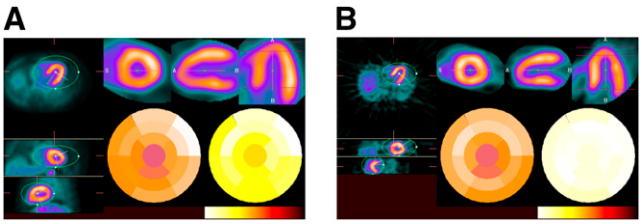

FIGURE 2. Transverse, coronal, and sagittal slices (left) as well as short-axis, long-vertical-axis, and horizontal-axis images (top right) of ^{82}Rb (A) and ^{13}N-ammonia (B) stress studies in same subject. Polar maps of relative perfusion (center) and absolute hyperemic MBF (right) are also shown (bottom right); white corresponds to highest values in color scale.

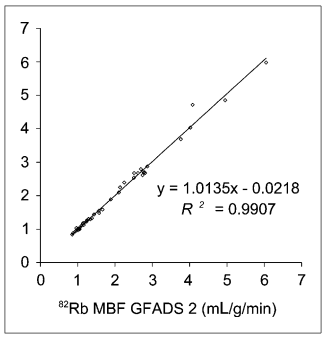

FIGURE 3. Intraobserver and GFADS variability of estimation of rest MBF and stress MBF with ^{82}Rb. Mean values for flow from 4 repeated estimates are shown for one observer.

estimation of MBF and CFR was also very good, with correlation coefficients of greater than 0.87. Similar results were obtained for the estimation of MBF at rest and MBF during stress.

Table 5 shows the Spearman ρ nonparametric correlations. All of the correlations were greater than 0.827 and statistically significant at the 0.01 level (2-tailed test). Finally, the intraclass correlation coefficients, reflecting the variability of different MBF measurements in the same subject relative to the total variation across all MBF measurements and all observers, were 0.8271 for rest ^{82}Rb MBF estimates (lower limit, 0.7419; upper limit, 0.8934) and 0.9058 for stress ^{82}Rb MBF estimates (lower limit, 0.8552; upper limit, 0.9432). The corresponding interobserver reliability coefficients were 0.950 at rest and 0.975 during peak stress.

Reproducibility of ^{82}Rb PET Estimates of MBF

Figure 5 shows the correlations between MBF estimates obtained for the 3 main coronary territories (LAD, LCX, and RCA) at rest and during peak stress in repeated ^{82}Rb studies as well as the corresponding Bland–Altman plots. The reproducibility of MBF estimates (R^2 = 0.935) and that of CFR estimates (R^2 = 0.841) were very good. Furthermore, the slope of the correlation line was not significantly different from one when estimating MBF (slope, 0.986) or CFR (slope, 0.960) in repeated ^{82}Rb studies. The coefficients of repeatability computed from the Bland–Altman plots were 15.2% for rest MBF and 16.0% for stress MBF and CFR. Furthermore, almost all differences between estimates obtained at visit 1 and those obtained at visit 2 were within the mean ± 1.96 SDs for both rest MBF and stress MBF, and no absolute systematic error was observed.

Accuracy of ^{82}Rb PET Estimates of MBF

Figure 6 shows the correlations between MBF estimates obtained for the 3 main coronary territories at rest and during peak stress in ^{82}Rb and ^{13}N-ammonia studies. Very good correlations were obtained between the ^{82}Rb studies and the ^{13}N-ammonia studies (R^2 = 0.857) for MBF ranging from 0.5 to 3 mL/g/min. The Bland–Altman plots revealed no significant proportional error for rest MBF or stress MBF and no dependence of the variations on the amplitude of MBF at rest or during stress. Furthermore, virtually all differences between estimates obtained with ^{13}N-ammonia and those obtained with ^{82}Rb were within the mean ± 1.96 SDs for both rest MBF and stress MBF. Compared with ^{13}N-ammonia, ^{82}Rb resulted in a small systematic overestimation of MBF at rest (0.129 mL/g/min) and an underestimation of MBF during stress (0.22 mL/g/min). The overall error was an underestimation of MBF of 0.04 mL/g/min by ^{82}Rb compared with ^{13}N-ammonia.

The correlation between CFR estimates obtained with ^{13}N-ammonia and ^{82}Rb was slightly lower (R^2 = 0.633)

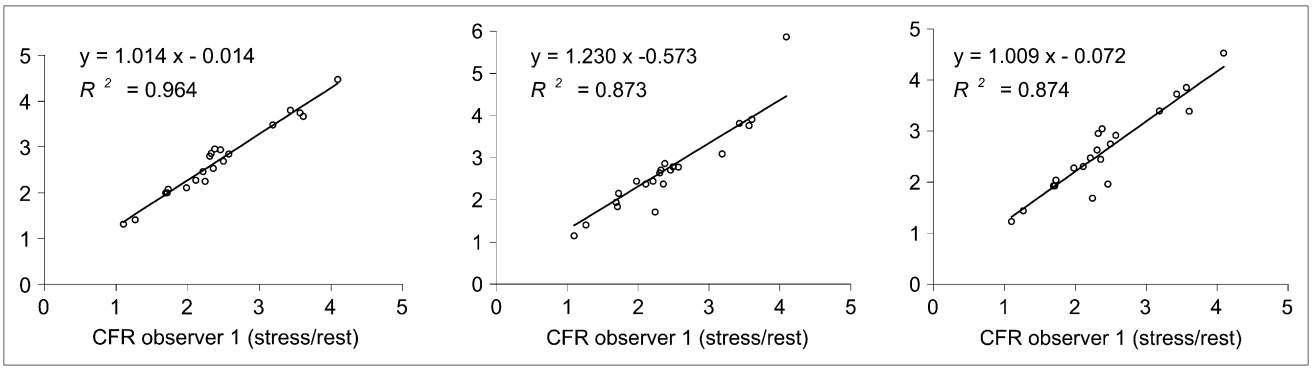

FIGURE 4. Interobserver variability of estimation of CFR with ^{82}Rb.

TABLE 5. Spearman ρ Nonparametric Correlations Among ^{82}Rb PET Estimates of MBF Obtained by 4 Observers

Spearman ρ	Observer 1	Observer 2	Observer 3	Observer 4
Observer 1	1.000	0.935*	0.845*	0.857*
Observer 2	0.935*	1.000*	0.891*	0.890*
Observer 3	0.845*	0.891*	1.000	0.827*
Observer 4	0.857*	0.890*	0.827*	1.000

*Correlation was significant at 0.01 level (2-tailed test).

than that for MBF, with CFR values ranging from 1 to 4.5. This finding was not unexpected because errors in the estimation of MBF at rest or stress will tend to magnify errors in the estimation of CFR (because CFR is calculated as peak MBF during stress/MBF at rest). Furthermore, the Bland–Altman plots for CFR revealed no significant proportional error and no dependence of the variations on the amplitude of CFR for values between 1 and 4.5. Furthermore, all differences between CFR estimates obtained with

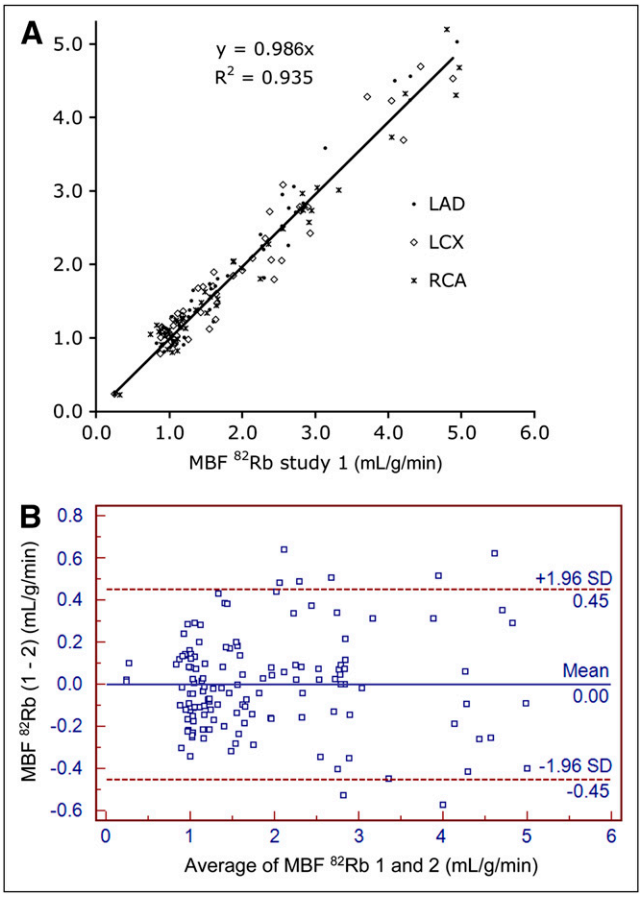

FIGURE 5. Reproducibility of rest MBF and stress MBF estimated with ^{82}Rb at 2 visits. (A) Correlation plot of 2 MBF measurements. (B) Bland–Altman plot of 2 MBF measurements.

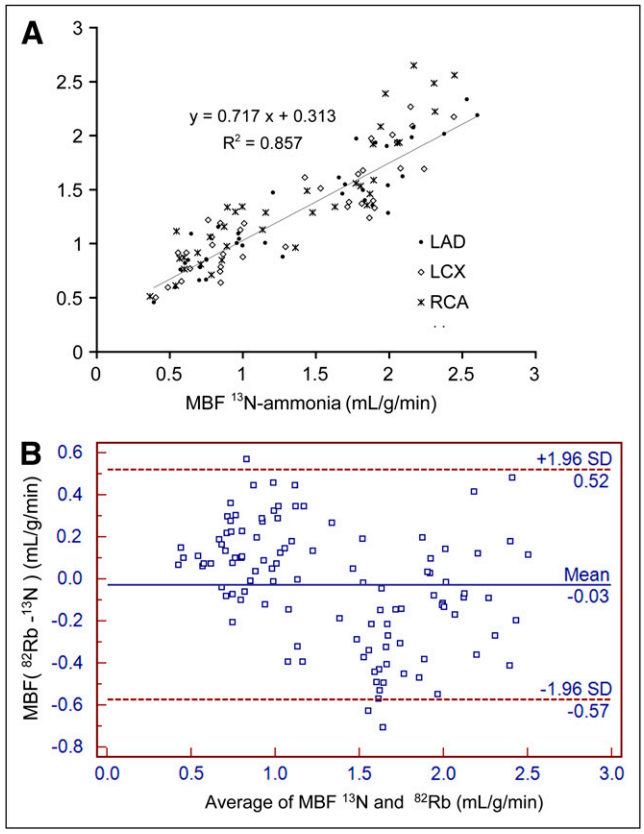

FIGURE 6. Comparison of rest MBF and stress MBF estimated with ^{82}Rb and ^{13}N-ammonia. (A) Correlation plot of ^{82}Rb and ^{13}N-ammonia MBF measurements. (B) Bland–Altman plot of ^{82}Rb and ^{13}N-ammonia MBF measurements. Bland–Altman plot illustrates slight overestimation of MBF at rest and underestimation during peak stress with ^{82}Rb compared with ^{13}N-ammonia.

^{13}N-ammonia and ^{82}Rb were within the mean ± 1.96 SDs. A systematic underestimation of CFR was observed with ^{82}Rb (0.58), presumably because of the smaller extraction fraction of ^{82}Rb.

These results were consistent with the results of paired Student t tests performed on MBF values obtained with ^{82}Rb and ^{13}N-ammonia. At rest, there was no significant difference at $P < 0.05$ in the LAD ($t = 1.5$) and the LCX ($t = 1.1$), but there was a small significant difference in the RCA ($t = 2.6$). During stress, there was no significant difference between MBF values obtained with ^{82}Rb and ^{13}N-ammonia in the LCX ($t = 2.1$) and the RCA ($t = 0.5$), but there was a marginal significant difference in the LAD ($t = 2.3$).

DISCUSSION

The detection of coronary artery stenosis and the evaluation of its physiologic significance (i.e., myocardial ischemia) have remained the central paradigms of the diagnosis and management of CAD. Myocardial perfusion imaging represents a robust approach to diagnosing ob-

structive CAD, quantifying the magnitude of jeopardized myocardium, and assessing the extent of myocardial viability. However, this approach often uncovers only the territory supplied by the most severe coronary artery stenosis and is inadequate to define the presence of multivessel CAD or diffuse microvascular dysfunction; these limitations may explain the paradoxical underestimation of clinical risk by a normal scan pattern in high-risk cohorts (e.g., subjects with diabetes). These limitations are widely recognized and apply to both SPECT and PET. The absolute quantification of MBF has been proposed as a possible solution to the underestimation of jeopardized myocardium by stress myocardial perfusion imaging. Previous studies suggested that the absolute quantification of regional myocardial perfusion (in mL/min/g) with ^{82}Rb is feasible. However, there are very few data on the accuracy and reproducibility of such measurements, which represent the main focus of the present study.

We used the GFADS approach (*14*) to estimate noninvasively the LV and RV input functions from the dynamic ^{82}Rb and ^{13}N-ammonia PET studies, and we used these estimates in the subsequent kinetic analysis. After fitting of the time-varying factor model to the dynamic data with a least squares objective function, a different objective function that penalized spatial overlap between factor images was minimized. Our approach does not require a priori knowledge of kinetics and can be used in other dynamic imaging applications, such as imaging with ^{15}O-water. Furthermore, our approach does not require drawing of volumes of interest to obtain LV and RV input functions. This feature is a major advantage because it obviates manual intervention in the quantitation scheme and makes the approach reproducible in the clinical setting. Although the number of factors must be defined before GFADS is performed, we found that $P = 3$ always yielded robust estimates of LV and RV input functions in all patient studies included in this work, as well as in more than 500 patient studies performed in our clinic. This finding is consistent with the fact that the first 3 eigenvectors obtained by principal components analysis were consistently several times higher than the other eigenvectors.

Ideally, GFADS provides independent factor images of the LV, RV, and myocardium. Therefore, kinetic model fitting with the blood time–activity curves derived from GFADS should essentially subtract the influence of LV and RV blood from the myocardial contribution, making a partial-volume correction for spillover unnecessary with our approach. Therefore, spillover attributable to myocardial contamination by the input function or to cardiac motion translates into an overestimation of f_v^i and r_v^i but not of k_1 or k_2. The fitting of r_v for all myocardial territories comes at the cost of a potential increase in the variance of this fit because some territories are not affected by RV spillover. In the compartment model, spillover from tissues was ignored for myocardial curves. Spillover to LV and RV from surrounding tissue is likely to be minimal because geometrically LV and RV are separated from surrounding tissue by the myocardium. Furthermore, we did not model spillover from lung tissue because lung retention of ^{82}Rb was previously reported by Chow et al. (*27*) to be very low (myocardial-to-lung activity ratio, 12:1). Such high values suggest a very low lung retention compared with myocardial retention and make lung spillover negligible. Spillover from the myocardium into the lung, on the other hand, may result in an underestimation of myocardial tissue concentration, which in turn may affect MBF quantification. Note that lung retention is much greater in ^{13}N-ammonia cardiac PET than in ^{82}Rb cardiac PET, especially in people who smoke and in patients with a low ejection fraction.

Our results show that estimation of MBF with dynamic ^{82}Rb PET is highly reproducible when generalized factor analysis is used to semiautomatically estimate LV and RV input functions and regional compartment analysis while modeling the extraction fraction for ^{82}Rb as a function of flow over a wide range of MBF values (0.7–5 mL/g/min). Our results are consistent with our previous findings (*14*) showing that reproducibility in realistic Monte Carlo simulations of MBF estimation with image-based estimation of input functions with GFADS and compartment modeling was substantially and significantly better than that of manual drawing of small regions of interest over the LV and RV regions of the reconstructed volumes followed by compartment modeling. The high reproducibility of MBF quantitation was achieved by requiring minimal intervention from the observer that consisted in delineating the large volume of study that encompasses the heart where all analyses were performed. No statistical differences were observed in any coronary territory in repeated ^{82}Rb studies at rest or during peak stress. This finding is consistent with results previously reported by Nagamachi et al. in the case of ^{13}N-ammonia (*28*). The excellent interstudy reproducibility with ^{82}Rb is comparable to that reported for ^{13}N-ammonia (~11%) by Nagamachi et al. (*28*). We also observed excellent intra- and interobserver reliability of our quantitative approach, which is likely related to the fact that it requires minimal observer intervention.

We have shown that the GFADS approach used in this study to estimate noninvasively the LV and RV input functions from the dynamic ^{82}Rb and ^{13}N-ammonia PET studies is highly reproducible (*14*). After fitting the time-varying factor model to the dynamic data using a least squares objective function, a different objective function which penalized spatial overlap between factor images was minimized. Our approach does not require a priori knowledge of kinetics and can be used with other radiotracers. Furthermore, our approach does not require drawing of volumes of interest to obtain LV and RV input functions. This feature is a major advantage because it obviates manual intervention in the quantitation algorithm and likely is responsible for the excellent results in the reproducibility analysis presented in this study. Although the number of factors must be defined before performing GFADS, we have found that $P = 3$

always yielded robust estimates of LV and RV input functions in all patient studies included in this work. This is consistent with the fact that the first 3 eigenvectors obtained by principal components analysis were consistently several times greater than the other eigenvectors.

Our results show that ^{82}Rb flow estimates correlated very well with ^{13}N-ammonia flow estimates for flow values that ranged from 0.5 to 2.5 mL/g/min. We observed a small systematic overestimation of rest MBF (0.129 mL/g/min) and an underestimation of stress MBF (0.22 mL/g/min) with ^{82}Rb. Several authors have measured the ^{82}Rb extraction fraction in animal models (*21,29,30*), and we have previously reported reasonable agreement among these models over the flow range of interest for healthy subjects and patients with mild CAD (e.g., $1 \leq$ flow ≤ 3.5 mL/g/min), as is the case in our present work (*31*). Nonetheless, the inaccuracies in the estimation of MBF with ^{82}Rb compared with ^{13}N-ammonia, especially during peak stress, may be related to the lower extraction of ^{82}Rb and the difficulties with its modeling as well as the lack of modeling of veinous egress.

In the accuracy study, systolic and mean arterial blood pressures and RPP tended to be lower when the subjects underwent the ^{13}N-ammonia study. These differences are most likely related to the sequence of the 2 scans, which for logistical reasons included the ^{82}Rb study before the ^{13}N-ammonia evaluation in most of the subjects. In addition, the fact that subjects were studied at 2 different hospitals, with potential differences in scanner room temperature and other factors, may have also contributed to the observed differences in resting hemodynamic parameters. Nonetheless, resting MBF was normalized to the RPP to account for within-group (reproducibility and accuracy) differences in resting cardiac work.

Despite our best efforts, we had few patients with documented CAD and none with evidence of stress perfusion defects. Furthermore, our extraction fraction model was not validated in a pathologic situation. Thus, our findings regarding the reproducibility and accuracy of MBF estimates with ^{82}Rb cannot be readily extrapolated to areas of low or very low blood flow (e.g., myocardial infarction). However, these areas of low blood flow are readily identifiable on visual or circumferential profile analyses. Thus, it is unlikely that absolute quantification of MBF would enhance diagnosis or risk assessment based on flow estimates in areas of obvious stress-induced ischemia or infarction.

CONCLUSION

Absolute quantitation of MBF with ^{82}Rb dynamic cardiac PET is reproducible and accurate compared with ^{13}N-ammonia. The reproducibility of the quantitative approach itself, as assessed by the intra- and interobserver reliability and that of repeated ^{82}Rb studies, was very good, with slopes of the correlation lines very close to unity. The correlation between MBF estimates obtained at rest and during peak stress with ^{82}Rb and ^{13}N-ammonia studies was also very good, with no significant proportional error and no dependence of variations on the amplitude of the MBF over the range of MBF values considered in the study.

ACKNOWLEDGMENTS

This work was supported in part by grants from the National Institutes of Health (RO1-EB005876) and the American Heart Association (GIA-655909T) and by an unrestricted educational Bracco Diagnostics grant. The contents of this article are the responsibility of the authors and do not represent the views of the National Institutes of Health or the American Heart Association.

REFERENCES

1. Kuhle W, Porenta G, Huang S-C, et al. Quantification of regional myocardial blood flow using ^{13}N-ammonia and reoriented dynamic positron emission tomographic imaging. *Circulation.* 1992;86:1004–1017.
2. Muzik O, Beanlands RS, Hutchins GD, Mangner TJ, Nguyen N, Schwaiger M. Validation of nitrogen-13-ammonia tracer kinetic model for quantification of myocardial blood flow using PET. *J Nucl Med.* 1993;34:83–91.
3. Nitzsche EU, Choi Y, Czernin J, Hoh CK, Huang SC, Schelbert HR. Noninvasive quantification of myocardial blood flow in humans: a direct comparison of the [^{13}N]ammonia and the [^{15}O]water techniques. *Circulation.* 1996;93:2000–2006.
4. Knesaurek K, Machac J, Krynyckyi BR, Almeida OD. Comparison of 2-dimensional and 3-dimensional ^{82}Rb myocardial perfusion PET imaging. *J Nucl Med.* 2003;44:1350–1356.
5. deKemp RA, Ruddy TD, Hewitt T, Dalipaj MM, Beanlands RSB. Detection of serial changes in absolute myocardial perfusion with ^{82}Rb PET. *J Nucl Med.* 2000;41:1426–1435.
6. Chen EQ, MacIntyre WJ, Fouad FM, et al. Measurement of cardiac output with first-pass determination during rubidium-82 PET myocardial perfusion imaging. *Eur J Nucl Med Mol Imaging.* 1996;23:993–996.
7. Dahl J, Muzik O, Wolfe ER, Allman C, Hutchins G, Schwaiger M. Myocardial rubidium-82 tissue kinetics assessed by dynamic positron emission tomography as a marker of myocardial cell membrane integrity and viability. *Circulation.* 1996;93:238–245.
8. Herrero P, Markham J, Shelton ME, Weinheimer CJ, Bergmann SR. Noninvasive quantification of regional myocardial perfusion with rubidium-82 and positron emission tomography: exploration of a mathematical model. *Circulation.* 1990; 82:1377–1386.
9. Gould KL. Clinical cardiac PET using generator-produced Rb-82: a review. *Cardiovasc Intervent Radiol.* 1989;12:245–251.
10. Gould KL, Goldstein RA, Mullani NA, et al. Noninvasive assessment of coronary stenoses by myocardial perfusion imaging during pharmacologic coronary vasodilation. VIII. Clinical feasibility of positron cardiac imaging without a cyclotron using generator-produced rubidium-82. *J Am Coll Cardiol.* 1986;7:775–789.
11. Schenker MP, Dorbala S, Hong EC, et al. Relationship between coronary calcification, myocardial ischemia, and outcomes in patients with intermediate likelihood of coronary artery disease. *Circulation.* 2007;116:S509–S510.
12. Di Carli MF, Dorbala S, Meserve J, El Fakhri G, Sitek A, Moore SC. Clinical myocardial perfusion PET/CT. *J Nucl Med.* 2007;48:783–793.
13. Lin JW, Sciacca RR, Chou RL, Laine FA, Bergmann SR. Quantification of myocardial perfusion in human subjects using ^{82}Rb and wavelet-based noise reduction. *J Nucl Med.* 2001;42:201–208.
14. El Fakhri G, Sitek A, Guérin B, Kijewski MF, Di Carli MF, Moore SC. Quantitative dynamic cardiac ^{82}Rb PET imaging using generalized factor and compartment analyses. *J Nucl Med.* 2005;46:1264–1271.
15. Burger C, Goerres G, Schoenes S, Buck A, Lonn AHR, von Schulthess GK. PET attenuation coefficients from CT images: experimental evaluation of the transformation of CT into PET 511-keV attenuation coefficients. *Eur J Nucl Med Mol Imaging.* 2002;29:922–927.
16. Bergstrom M, Eriksson L, Bohm C, Blomqvist G, Litton J. Correction for scattered radiation in a ring detector positron camera by integral transformation of the projections. *J Comput Assist Tomogr.* 1983;7:42–50.

17. El Fakhri G, Sitek A, Di Carli MF. QDA: an automated graphical software for absolute quantification of regional myocardial blood flow [abstract]. *J Nucl Med.* 2007;48:203.
18. Sitek A, Gullberg GT, Huesman RH. Correction for ambiguous solutions in factor analysis using a penalized least squares objective. *IEEE Trans Med Imaging.* 2002;21:216–225.
19. Cerqueira MD, Weissman NJ, Dilsizian V, et al. Standardized myocardial segmentation and nomenclature for tomographic imaging of the heart: a statement for healthcare professionals from the Cardiac Imaging Committee of the Council on Clinical Cardiology of the American Heart Association. *J Nucl Cardiol.* 2002;9:240–245.
20. Gould KL. *Coronary Artery Stenosis and Reversing Atherosclerosis.* 2nd ed. London, U.K.: Arnold; 1999:247–273.
21. Yoshida K, Mullani N, Gould KL. Coronary flow and flow reserve by PET simplified for clinical applications using rubidium-82 or nitrogen-13-ammonia. *J Nucl Med.* 1996;37:1701–1712.
22. Leader JL. *Numerical Analysis and Scientific Computation.* Boston, MA: Pearson Addison Wesley; 2004.
23. Press WH, Teukolsky SA, Vettering WT, Flannery BP. *Numerical Recipes in C: The Art of Scientific Computing.* 2nd ed. Cambridge, U.K.: Cambridge University Press; 1992.
24. Kendall MG, Stuart A. *The Advanced Theory of Statistics.* London, U.K.: Griffin; 1979.
25. Bland JM, Altman DG. Statistical methods for assessing agreement between two methods of clinical measurement. *Lancet.* 1986;1:307–310.
26. Bland JM, Altman DG. Measuring agreement in method comparison studies. *Stat Methods Med Res.* 1999;8:135–160.
27. Chow BJW, Ananthasubramaniam K, deKemp RA, Dalipaj MM, Beanlands RSB, Ruddy TD. Comparison of treadmill exercise versus dipyridamole stress with myocardial perfusion imaging using rubidium-82 positron emission tomography. *J Am Coll Cardiol.* 2005;45:1227–1234.
28. Nagamachi S, Czernin J, Kim AS, et al. Reproducibility of measurements of regional resting and hyperemic myocardial blood flow assessed with PET. *J Nucl Med.* 1996;37:1626–1631.
29. Mullani NA, Goldstein RA, Gould KL, et al. Myocardial perfusion with rubidium-82. I. Measurement of extraction fraction and flow with external detectors. *J Nucl Med.* 1983;24:898–906.
30. Marshall RC, Taylor SE, Powers-Risius P, et al. Kinetic analysis of rubidium and thallium as deposited myocardial blood flow tracers in isolated rabbit heart. *Am J Physiol.* 1997;272:H1480–H1490.
31. Moore SC, El Fakhri G. Principles of quantitation in cardiac PET. In: Di Carli MF, Lipton MJ, eds. *Cardiac PET and PET/CT Imaging.* New York, NY: Springer; 2007:46–70.

JNM The Journal of NUCLEAR MEDICINE

Reproducibility and Accuracy of Quantitative Myocardial Blood Flow Assessment with ^{82}Rb PET: Comparison with ^{13}N-Ammonia PET

Georges El Fakhri, Arash Kardan, Arkadiusz Sitek, Sharmila Dorbala, Nathalie Abi-Hatem, Youmna Lahoud, Alan Fischman, Martha Coughlan, Tsunehiro Yasuda and Marcelo F. Di Carli

J Nucl Med. 2009;50:1062-1071.
Published online: June 12, 2009.
Doi: 10.2967/jnumed.104.007831

The Journal of Nuclear Medicine is published monthly.
SNMMI | Society of Nuclear Medicine and Molecular Imaging
1850 Samuel Morse Drive, Reston, VA 20190.
(Print ISSN: 0161-5505, Online ISSN: 2159-662X)

SNMMI SOCIETY OF NUCLEAR MEDICINE AND MOLECULAR IMAGING